Available online at www.sciencedirect.com

ScienceDirect

Procedia CIRP 117 (2023) 432–437

www.elsevier.com/locate/procedia

19th CIRP Conference on Modeling of Machining Operations

A Novel 2D Micromilling FEM simulation strategy to optimize the flow stress law of IN625.

Andrea Abeni[a]*, Cristian Cappellini[b], Aldo Attanasio[a]

[a]*University of Brescia, Via Branze 38, Brescia 25123, Italy*
[b]*University of Bergamo, Via Pasubio 7/b, Dalmine 24044, Italy*

* Corresponding author. Tel.: +39-030-3711212; fax: +39-030-3712448. *E-mail address:* andrea.abeni@unibs.it

Abstract

The products miniaturization tendency of the last years led to an acceleration of micromilling process development. Considering the high-quality requirements, a deep knowledge of this operation, concerning ploughing-shearing transition, tool run-out, and tool edge radius effects, is mandatory, especially when machining difficult-to-cut materials. For this reason, this paper introduces a novel 2D micromachining Finite Element Method simulation strategy for micromilling forces evaluation, when cutting IN625. The major output of this technique consists in the computation of an optimized flow stress law, suitable for the simulation of high-speed machining. Particle Swarm Optimization method was employed for optimizing the flow stress parameters by comparing the cutting force predicted by an analytical model previously calibrated on experimental data, providing good agreement. This strategy permits the micromilling process predictive analysis, avoiding costly optimization experimental tests.

Keywords:

1. Introduction

The increasing request of green manufacturing and sustainability to which the industrial field must comply in the contemporary era, led to a boost in weight and volume reduction of components [1]. Effective responses to this need have been recognized in miniaturization and topological optimization [2]. Amongst the emerging technologies granting these achievements, the most disruptive is represented by additive manufacturing (AM), ensuring the production of complex shaped parts, even of micrometric dimensions, in several industries, such as mechanical [3], aerospace [4], and automotive [5]. Moreover, this technique permits to process high performance materials difficult to be managed with conventional processes [6]. On the other hand, the surface quality achievable by AM is often lower than required, hence a finishing process is needed. When facing with micro-components, for assessing the proper quality, micromilling is one of the processes that can be succesfully employed. Due to the ploughing-shearing cutting transition mechanism, tool run-out, and tool edge radius effects to which this process is prone, especially when working with hard-to-cut materials, a profound awareness of how these affect quality, tool wear, and cutting forces is fundamental. Finite Element Method (FEM) simulations demonstrated to be a proficient methodology for predicting these correlations [7,8]. FEM reliability is subjected to its correct setup, concerning the implementation of cutting parameters, friction, material behavior, characterized by flow stress law.

This paper proposes a novel 2D FEM simulation setup, able to forecast machining forces, when micromilling additive manufactured Inconel625 (IN625) specimens. Starting from the comparison of the simulated cutting forces with the ones calculated by means of a force analytical model, previously

10.1016/j.procir.2023.03.073

validated by experimental measures, the parameters of a modified Johnson-Cook (J-C) flow stress law were calibrated by applying a Particle Swarm Optimization (PSO) algorithm [9]. The good agreement amongst FEM and model results implies the predictive capability of the proposed methodology. The development of a numerical model appears profitable due to the possibility to predict more outputs if compared with the analytical model. On other limit of the analytical modeling approach is that it is suitable only for orthogonal cutting of thin-walled samples. Otherwise, FEM can be easily employed with more complex configuration of cutting. Once the procedure described in this paper is applied to calibrate flow stress in this simplified configuration, the flow stress can be utilized to predict cutting forces in generic micro-machining.

2. Materials and Methods

In order to validate the proposed 2D FEM methodology, the optimization of the material flow stress, by the selection of the most suitable plastic behavior law and the calibration of the related coefficient, is mandatory. This latter was performed by the comparison of peak cutting forces between a previously verified analytical model [10] and simulated values. A brief description of the experimental campaign and the derived cutting force analytical model is presented in Section 2.1, while Sections 2.2 and 2.3 sequentially explain the FEM setup, and the material flow stress optimization procedure.

2.1. Experimental campaign

The micromilled specimens were produced by LaserCUSING™, a patented version of Selective Laser Melting (SLM) process, of IN625 powders, whose chemical composition is reported in Table 1. The employed process parameters were a laser power of 370 W, a scanning speed of 1200 mm/s, a laser spot size of 170 µm, a layer thickness of 60 µm, a hatch distance of 110 µm, a stripe width of 5 mm, and an energy density of 46.7 J/mm³. As visible in (Figure 1), 12 thin walls 0.2 mm thick were created on each specimen.

Table 1. IN625 chemical composition.

Element	Ni	Cr	Mo	C	Fe	Si	Al	Ti
wt(%)	61.6	22.0	9.0	4.0	3.0	<0.3	<0.2	<0.2

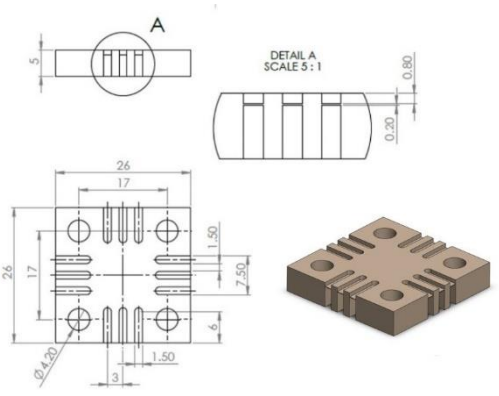

Fig. 1. Geometry of the specimens utilized in the experimental campaign.

The micromilling tests were then performed on a five axis nano-precision machining center KERN Pyramid Nano, by cutting the thin walls with a 2-flutes micro-end mill tools (Figure 2b), whose characteristics are summarized in Table 2. Each cutting test was achieved without engaging the tool bottom and moving it from the outside to the center, realizing a slot in the thin wall with a length of 5 mm (Figure 2a).

Three repetitions of the combination of three different values of the feed rate f_Z [µm/tooth*rev] with two distinct cutting speeds V_C [m/min], by maintaining a constant depth of cut a_p of 0.2 mm (thin wall thickness), were performed, giving a total number of 18 micromilling tests.

Table 2. Characteristics of the employed micro-end mill tool.

Feature	Value
Model code	103L008R005-MEGA-64-T
Effective diameter [µm]*	789±3
Cutting edge radius [µm]	4
Helix angle [°]	0
Material	Tungsten Carbide (WC)
Coating material	Titanium Nitride (AlTiN)

*measured by Hirox RH2000 optical microscope

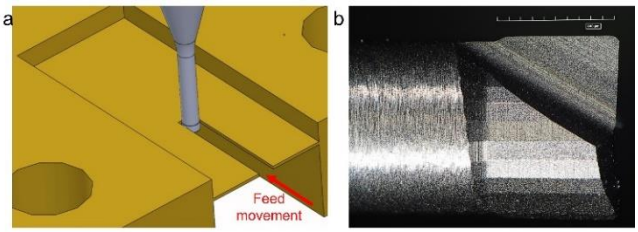

Fig. 2. (a) Cutting test process methodology; (b) employed micro-end mill.

Cutting forces F_C were acquired by means of the measurement system described in [10]. A portion of signal corresponding to thirty tool rotations was extrapolated and averaged to compute the average peak of cutting force $F_{C\,max}$ for each repetition of each test. The analytical model of F_C considers both the shearing and ploughing cutting regime. It is based on the instantaneous uncut chip thickness $h(\theta)$ and ploughed cutting area $A_p(\theta)$ along the tool rotational angle θ. Both $h(\theta)$ and $A_p(\theta)$ are, in turn, function of f_Z and V_C. θ is expressed as the product amongst the rotational speed ω and the time t, as reported in Equation (1):

$$F_t(\theta) = \left(K_{ts} * h(\theta) + K_{tp} * A_p(\theta)\right) * a_p$$
$$F_r(\theta) = \left(K_{rs} * h(\theta) + K_{rp} * A_p(\theta)\right) * a_p \quad | \ \theta = \omega \cdot t \tag{1}$$

Where F_t and F_r are the tangential and radial components of F_C respectively, K_{ts} = 2595 MPa and K_{tp} = 4625 MPa are the values of the shearing and ploughing coefficients for F_t, while K_{rs} = 1870 MPa and K_{rp} = 3000 MPa are the ones concerning F_r (taken from the validated analytical model of [10]). Their composition allows to estimate F_C during θ as a function of the cutting parameters, Equation (2).

$$F_C(\theta) = \sqrt{[F_t(\theta)^2 + F_r(\theta)^2]} \tag{2}$$

Table 3. Experimental cutting forces of the executed micromilling tests.

Test	f_Z [µm/tooth*rev]	V_C [m/min]	$F_{C\,max\,Exp}$ [N]	$F_{C\,max\,An}$ [N]	$e_{\%}$
A	2.5	30	2.143	2.197	2.5
B	2.5	40	2.297	2.340	1.9
C	5.0	30	3.430	3.070	10.5
D	5.0	40	3.547	3.103	12.5
E	10.0	30	5.510	5.617	1.9
F	10.0	40	5.217	5.270	1.0

Table 3 reports the cutting parameters of the performed tests, the related experimental and calculated values, obtained by Equation (2), of the maximum value of the cutting forces, and the estimation errors [10]. Due to the low values of the errors, this model can be profitably employed for the succeeding comparison with the simulated cutting forces. The usage of the cutting force computed by analytical model as benchmark instead of the experimental data, allows to generate analytical force data in a wide range of process parameters, without the necessity to perform time-consuming and costly experimental tests.

2.2. FEM modeling

Considering the null value of the tool helix angle, 2D FEM simulations can be exploited for modeling purpose [7]. Therefore, the experimental tests were faithfully reproduced by thermomechanical simulations in the Deform2D® FEM environment. In order to correctly characterize the intrinsic chip thickness variation during the micromill rotation, as suggested in [11], the workpiece geometry was represented as a semi-tubular section having an internal boundary corresponding to the hypothetical trajectory of the previous cutting-edge passage, and a circular arc for the external boundary. The depth of cut was considered constant and equal to 0.2 mm. With the aim of reducing computational times, only the portion of the tool geometry closely in contact with the workpiece was considered. Figure 3 shows the beginning of the proposed cutting simulation, where workpiece and tool geometry are visible.

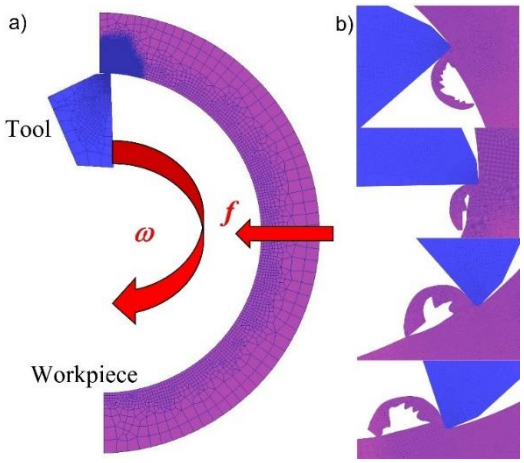

Fig. 3. FEM cutting simulation setup, a) overview, b) chip at different times.

Moreover, the cutting speed movement was assigned to the tool, by putting it into rotation around tool rotational axis, with a rotation speed ω [rad/s] corresponding to the desired V_C [m/min]; while the workpiece was moved against the tool with a feed rate f [mm/s] equivalent to the required f_Z [µm/tooth*rev], as reported in Table 4 in consideration of a micromill diameter of 789 µm.The tool was considered as a rigid object. For correctly estimating its temperature distribution during the process, the material thermal properties of WC from Deform database were assigned. It was discretized with a mesh consisting of 1500 quadrangular linear elements and a sequence of mesh windows providing an element size at the tool edge region lower than 0.5 µm. An elasto-plastic mechanical behavior was assigned to the workpiece. Temperature-dependent IN625 elastic and thermal properties derived from [12] were used. The plastic material behavior, described by flow stress, will be discussed in the Section 2.3. The workpiece was meshed with 15000 quadrangular linear elements, employing a dynamic mesh window following the tool movement, giving a minimum element size lower than 1 µm. A heat transfer coefficient, *htc* of 20 W/m^{2}K, with the environment, at a temperature of 20 °C, was defined for both tool and workpiece. The contact between the two objects, at the tool-chip interface, was defined by a shear model with a friction factor m of 0.6 and adopting a *htc* of 100000 W/m^{2}K [13].

Table 4. Cutting speed and feed rate implemented in the FEM models.

Test	f_Z [µm/tooth]	→	f [mm/s]	V_C [m/min]	→	ω [rad/s]
A	2.5	→	1.008	30	→	1267
B	2.5	→	1.345	40	→	1690
C	5.0	→	2.017	30	→	1267
D	5.0	→	2.689	40	→	1690
E	10.0	→	4.034	30	→	1267
F	10.0	→	5.379	40	→	1690

2.3. Flow stress modeling

The selected flow stress law $\sigma(\varepsilon,\dot{\varepsilon},T)$, implemented in the FEM environment, is the modified Johnson-Cook (J-C) model that is the typical one employed when simulating machining operation of nichel-chromium based alloys [14, 15]. It describes the plastic material behavior as a function of strain ε, strain rate $\dot{\varepsilon}$ [s^{-1}], temperature T [°C], and it is represented by Equation (3):

$$\sigma(\varepsilon,\dot{\varepsilon},T) = [A + B\varepsilon^n]\left[1 + C\,ln\left(\frac{\dot{\varepsilon}}{\dot{\varepsilon}_0}\right)\right]\left[1 - \left(\frac{T - T_r}{T_m - T_r}\right)^m\right]$$

$$\left[M + (1 - M)\left(tanh\left(\frac{1}{(\varepsilon + p)^r}\right)\right)^S\right] \quad (3)$$

Where $\dot{\varepsilon}_0$ [s^{-1}] is the reference strain rate, T_r and T_m [°C] are the environment and material melting temperatures respectively, while the other parameters are material related constants. As visible in Equation (3), the first three parts of it in squared backets are related to the effects of ε, $\dot{\varepsilon}$, and T on

the material plasticity, while the last one is a hyperbolic function permitting to correctly represents the chip segmentation [16, 17]. The material constants for IN625 proposed in [14] are reported in Table 5, while its behavior as a function of strain at different strain rates and temperatures is depicted in Figure 4. The trend of stress on the strain is was firstly proposed by Calamaz et at. [18] to simulate discontinuous chips in orthogonal cutting Ti-6Al-4V alloy without employing chip separation criterion.

Table 5. IN625 Johnson-Cook material constants from [14].

A [MPa]	B [MPa]	C	n	m	$\dot{\varepsilon}_0$ [s^{-1}]
559	3000	0.00021	0.5	2	1670
T_m [°C]	T_r [°C]	M	p	r	S
1350	20	0.2	0	0.65	10

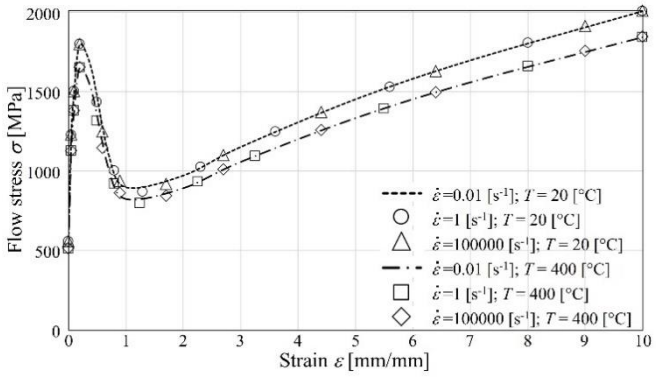

Fig. 4. σ_{Init} function of strain for different strain rate and temperature values.

With the intent of verifying the flow stress parameters of Table 5, an initial FEM simulation, truthfully reproducing Test E (V_C = 30 m/min; f_Z = 10 µm/tooth*rev), was setup following the novel methodology described in Section 2.2. For this reason, the flow stress derived from Table 5 parameters has been defined as σ_{Init}. The resulting cutting force during the tool rotation of this simulation was then compared with the one estimated by the analytical model of Equation (2), as reported in Figure 5.

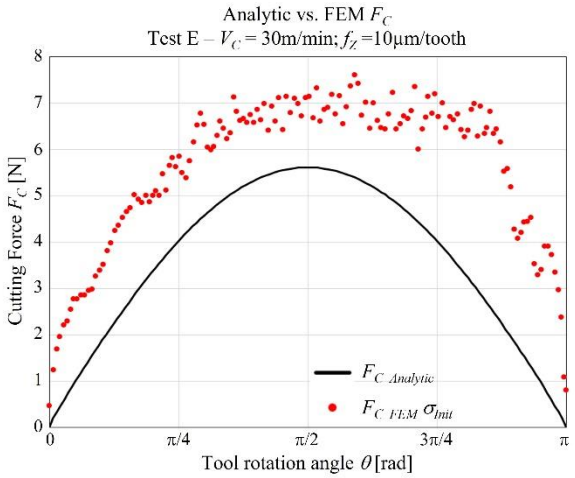

Fig. 5. Analytic and FEM F_C comparison by the implementation of σ_{Init}.

The evolution of the simulated cutting force, throughout the tool rotational angle, shows a trend that corresponds with the one predicted by the analytical model, enforcing the suitability of the proposed 2D FEM approach. On the contrary, the discrepancy of the F_C values is clearly observable. In particular, the F_C resulting from the simulation is greater than the analytical one. This can be ascribed to the fact that the parameters of σ_{Init} presented in [14] are derived from Hopkinson Split Bar tests of rolled and annealed material, that is characterized by different mechanical and physical properties respect to the specimens machined in this work, that were produced by AM process with intrinsic higher porosity and lower density. Therefore, to correctly estimate the cutting forces by simulation, an optimization of the J-C model's parameters is mandatory.

Equation (3) reveals that flow stress is defined by a total number of 12 parameters. A concurrent optimization of these all is a time and energy consuming iterative process. Hence, since each bracket-squared part has a determined significance in the material behavior description, for improving the optimization procedure, the following assumption have been made.

- The strain rate has a minimal effect on the material behavior, as demonstrated by the experimental data [10]. The low value of the C constant in the J-C model [14] was kept constant as in the original model.
- At high temperatures, IN625 alloys retain high mechanical characteristics, thus, flow stress curves remain close one to each other even when the temperature is varying, as observable in Figure 4. For this reason, the m parameter was maintained equal to 2, as proposed in [14].
- The hyperbolic function mainly affects the material softening behavior in the primary shear zone leading to the simulation of chip segmentation, but its effect on the cutting force peak is neglectable. Since the objective of this work is to correctly estimate F_C, the constants' values related to this part of the model were kept unchanged.

Subsequent to these assumptions, Equation (3) becomes:

$$\sigma(\varepsilon,\dot{\varepsilon},T) = [A + B\varepsilon^n]\left[1 + C\,ln\left(\frac{\dot{\varepsilon}}{\dot{\varepsilon}_0}\right)\right]\left[1 - \left(\frac{T-T_r}{T_m-T_r}\right)^2\right][F(tanh(\varepsilon))] \quad (4)$$

Where $F(tanh(\varepsilon))$ represents the unchanged hyperbolic function, and the only parameters need to be optimized are A, B and n.

The F_C peak values in Figure 5 are 5.617 N and 7.623 N for the analytic (F_{CMA}) and FEM (F_{CMF}) models respectively. The analytical cutting force peak was computed by considering the depth of cut of 0.2 mm. This leads to a percentage error $e_{\%}$ in the F_C estimation by FEM of 35.7 % (Equation (5)):

$$e_{\%} = \frac{|F_{CMA}-F_{CMF}|}{F_{CMA}} \cdot 100 = \frac{|5.617-7.623|}{5.617} \cdot 100 = 35.7\% \quad (5)$$

Assuming that material flow stress is the only factor influencing the cutting force prediction of the FEM model,

and considering the overestimation of the simulated forces, σ_{Init} was multiplied for a factor K defined in Equation (6), obtaining a new set of reduced flow stress curves to be tested and fitted.

$$K = 1 - e_{\%} = 1 - 0.357 = 0.643 \quad (6)$$

Several values of σ_{Init} were computed for a wide range of temperature, strain and strain rate and they were subsequently multiplied for K. For fitting the reduced flow stress values, an optimization of A, B and n parameters was performed by the application of the PSO algorithm. The error function $Err(\sigma)$ to be minimized was the normalized difference between K times σ_{Init} and the desired optimized flow stress law σ_{Opt}, for each strain and temperature, as defined in Equation (7):

$$Err(\sigma) = \sum_{i,j} \left(\frac{|K \cdot \sigma_{Init}(\varepsilon_i, T_j) - \sigma_{Opt}(\varepsilon_i, T_j)|}{K \cdot \sigma_{Init}(\varepsilon_i, T_j)} \right) \begin{matrix} i = 0 - 10[\frac{mm}{mm}] \\ j = 20 - 800[°C] \end{matrix} \quad (7)$$

σ_{Init} (Equation (3) with the parameters of Table 5), Equation (4) and Equation (7) were implemented in a Matlab® function. By the application of the PSO toolbox search algorithm, $Err(\sigma)$ was minimized by iteratively varying A, B and n values allowing their calibration. The optimization process was performed considering a population of 100 particles and 1000 iterations. The domains for A, B, C and n, were set to [300-800], [1000-4000] and [0.1-0.7] respectively. The calibrated values are $A = 415$, $B = 2229$, $n = 0.4998$. Therefore, the J-C model parameters of σ_{Opt} are the ones reported in Table 6. Figure 6 shows the comparison between σ_{Init} and the optimized flow stress σ_{Opt}.

Table 6. Optimized Johnson-Cook material constants for SLM IN625 (σ_{Opt}).

A [MPa]	B [MPa]	C	n	m	$\dot{\varepsilon}_0$ [s^{-1}]
415	2229	0.00021	0.4998	2	1670
T_m [°C]	T_r [°C]	M	p	r	S
1350	20	0.2	0	0.65	10

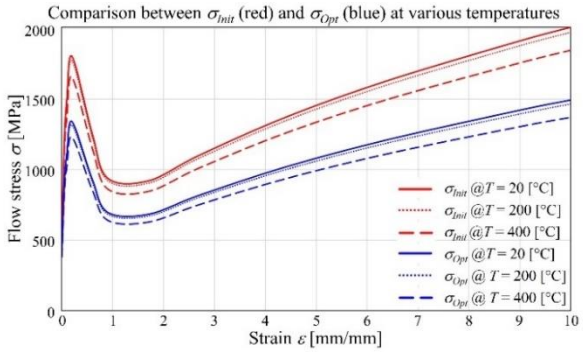

Fig. 6. Optimized and [14] flow stress comparison at different temperatures.

The optimized flow stress law σ_{Opt} (Equation (3) with parameters' values of Table 6) was then implemented in a FEM simulation reproducing Test E, giving encouraging results. As visible in the comparison amongst analytic and simulated F_C (Figure 7), both trend and module agree, with a $e_{\%}$ of peaks of 8.9 %.

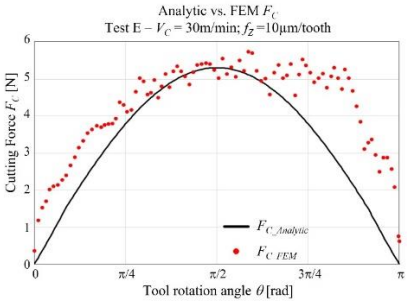

Fig. 7. Comparison between analytic and FEM F_C with σ_{Opt} for Test E.

3. Results

Following the FEM approach of Section 2.2, the validation of the simulation procedure and PSO optimized flow stress law was carried out by the comparison of analytic and FEM F_C peaks for the whole experimental tests.

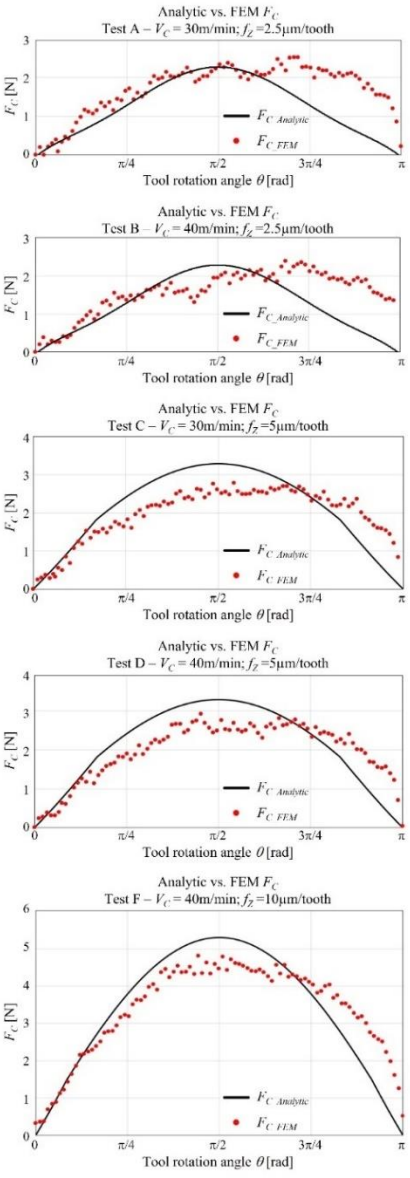

Fig. 8. Analytic and FEM F_C, with σ_{Opt}, comparison for tests A, B, C, D, F.

Figure 8 shows this comparison for tests A, B, C, D, and F respectively. The analytical cutting force signals were computed by considering the depth of cut of 0.2 mm. It is possible to appreciate the evolution of F_C along θ as well. Common to all the tests, is the higher amount of simulated F_C respect to the analytical one, at θ values closed to π, that represents a cutting-edge position nearby the disengagement from the workpiece. At this point, it can be experimentally observed [10] that $h(\theta)$ is tiny, conducting to a F_C reduction, as correctly described analytically. As visible in the bottom part of Figure 2b, instead, the simulation does not show this thickness reduction with a greater resulting F_C. This is due to a wrong evaluation of the chip segmentation. For solving this aspect, further studies should be done to optimize $F(\tanh(\varepsilon))$ in Equation (4). By increasing f_Z, the ploughing mechanism is lessened on behalf of the shearing one, making the FEM chip process generation closer to the experimental conditions, reducing F_C. For f_Z values of 2.5 and 10 µm/tooth, cutting at V_C=30m/min leads to higher FEM F_C than V_C=40m/min. This is ascribable to a lower cutting power and temperature when applying low V_C. Consequently, higher material properties are observed causing a F_C growth. The oscillation of the FEM F_C values respect to the analytic curve is related to the intrinsic features of numerical methods. Overall, the cutting force trends are in good agreement, confirming the reliability of the established 2D FEM technique and the validity of the flow stress law parameters optimized by PSO methodology. Table 7 reports the comparison of F_{CMA} and F_{CMF} peaks values with percentage errors. The low values of these latter indicate the capability of the implemented σ_{Opt} to correctly forecast the cutting forces.

Table 7. Analytic F_{CMA} and FEM F_{CMF} peak force comparison.

Test	F_{CMA} [N]	F_{CMF} [N]	$e_{\%}$
A	2.306	2.536	9.9
B	2.306	2.394	3.8
C	3.264	2.780	14.8
D	3.264	2.914	10.7
E	5.261	5.735	8.9
F	5.261	4.815	8.4

4. Conclusions and further studies

This paper presented a novel optimization technique of a modified Johnson-Cook flow stress law for simulating, by FEM, the micromilling of additive manufactured IN625 alloy parts. The parameters of the material flow stress model were optimized by means of a PSO algorithm. The derived material constitutive law was implemented in an original 2D FEM simulation setup in which the workpiece owned a geometry considering to the theoretical trajectory of the previous cutting-edge passage. The FEM forces were compared with the ones calculated by a previously validated analytic model, giving good superposition, in terms of forces' peaks and trends. Conversely, due to a not calibrated chip segmentation model, an overestimation of FEM loads was observed when tool is disengaging from workpiece. Therefore, to correctly represent forces in this last phase, further development of this work will be the optimization of chip breakage. Overall, the comparison between FEM and analytic results underlined the reliability of the proposed optimization methodology and the prediction capability of the FEM technique, furnishing a trustworthy tool and avoiding the needs of costly and time-consuming experimental tests.

References

[1] Gupta K, Gupta MK. Developments in nonconventional machining for sustainable production: A state-of-the-art review. Porc. Institut Mech Eng Part C J Mech Eng Sci 2019;233(12):4213-4232.

[2] Rosli AM, Jamaludin AS, Razali MNM. Recent study on hard to machine material – Micromilling process. Evergreen 2021;8(2):445-453.

[3] Concli F, Maccioni L, Fraccaroli L, Cappellini C. Effect of gear design parameters on stress histories induced by different tooth bending fatigue tests: A numerical-statistical investigation. Appl Sci 2022;12(8):3950.

[4] Madhavadas V, Srivastava D, Chadha U, Aravind RS, Sultan MTH, Shahar FS, Shah AUM. A review on metal additive manufacturing for intricately shaped aerospace components. CIRP J Manuf Sci Technol 2022;39:18-36.

[5] Rouf S, Raina A, Irfan UHM, Naveed N, Jeganmohan S, Farzana KA. 3D printed parts and mechanical properties: Influencing parameters, sustainability aspects, global market scenario, challenges and applications. Adv Ind Eng Polym Res 2022;5(3):143-158.

[6] Zhou R, Liu H, Wang H. Modeling and simulation of metal selective laser melting process: a critical review. Int J Adv Manuf Technol 2022;121(9-10):5693-5706.

[7] Cappellini C, Abeni A. Development and implementation of crater and flank tool wear model for hard turning simulations. Int J Adv Manuf Technol 2022;120(3-4):2055-2073.

[8] Abeni A, Ceretti E, Özel T, Attanasio A. FEM simulation of micromilling of CuZn37 brass considering tool run-out. Proc CIRP 2019, 82, 172-177.

[9] Eberhart R, Kennedy J. A new optimizer using particle swarm theory. Proc 6th Int Symposium Micro Machine and Human Science. Nagoja: IEEE; 1995:39-43.

[10] Abeni A, Loda D, Özel T, Attanasio A. Analytical force modelling for micro milling additively fabricated Inconel 625. Prod Eng 2020;14(5-6):613-627.

[11] Abeni A, Cappellini C, Ginestra PS, Attanasio A. Analytical modeling of micro-milling operations on biocompatible Ti6Al4V titanium alloy. Proc CIRP 2022;110:8-13.

[12] Wang Z, Denlinger E, Michaleris P, Stoica AD, Ma D, Beese AM. Residual stress mapping in Inconel 625 fabricated through additive manufacturing: Method for neutron diffraction measurements to validate thermomechanical model predictions. Mater Des 2017;113:169-177.

[13] Abeni A, Cappellini C, Attanasio A. Finite element simulation of tool wear in machining of nickel-chromiumbased superalloy. Proc ESAFORM 2021;4302. https://popups.uliege.be/esaform21/index.php?id=4302

[14] Hokka M, Leemet T, Shrot A, Bäker M, Kuokkala VT. Modelling of the dynamics behaviour of hard-to-machine alloys. EPJ Conf 201;226:04009.

[15] Arrazola PJ, Kortabarria A, Madariaga A, Esnaola JA, Fernandez E, Cappellini C, Ulutan D, Özel T. On the machining induced residual stresses in IN718 nickel-based alloy: experiments and predictions with finite element simulation. Simul Model Pract Theory 2014;41:87-103.

[16] Melkote SN, Grzesik W, Outeiro J, Rech J, Schulze V, Attia A, Arrazola PJ, M'Saoubi R, Saldana C. advances in material and friction data for modelling of metal machining. CIRP Ann Manuf Technol 2017;66:731-754.

[17] Farahani HK, Ketabchi M, Zangeneh S. Determination of Johnson-Cook plasticity model parameters for Inconel718. J Mat Eng Perf 2017;26(11):5284-5293.

[18] Calamaz M, Coupard D, Girot F. A new material model for 2D numerical simulation of serrated chip formation when machining titanium alloy Ti-6Al-4V. Int J Mach Tools Manuf 2008;48:275–288.